BIOCHEMISTRY
including biophysical chemistry & molecular biology

Article

pubs.acs.org/biochemistry

Tyrosine 110 Plays a Critical Role in Regulating the Allosteric Inhibition of *Campylobacter jejuni* Dihydrodipicolinate Synthase by Lysine

Cuylar J. T. Conly, Yulia V. Skovpen, Shuo Li, David R. J. Palmer,* and David A. R. Sanders*

Department of Chemistry, University of Saskatchewan, 110 Science Place, Saskatoon, SK S7N 5C9, Canada

ABSTRACT: Dihydrodipicolinate synthase (DHDPS), an enzyme found in most bacteria and plants, controls a critical step in the biosynthesis of L-lysine and *meso*-diaminopimelate, necessary components for bacterial cell wall biosynthesis. DHDPS catalyzes the condensation of pyruvate and (*S*)-aspartate-*β*-semialdehyde, forming an unstable product that is dehydrated to dihydrodipicolinate. The tetrameric enzyme is allosterically inhibited by L-lysine, and a better understanding of the allosteric inhibition mechanism is necessary for the design of potent antibacterial therapeutics. Here we describe the high-resolution crystal structures of DHDPS from *Campylobacter jejuni* with and without its inhibitor bound to the allosteric sites. These structures reveal a role for Y110 in the regulation of the allosteric inhibition by lysine. Mutation of Y110 to phenylalanine results in insensitivity to lysine inhibition, although the mutant crystal structure reveals that lysine does bind in the allosteric site. Comparison of the lysine-bound Y110F structure with wild-type structures reveals that key structural changes due to lysine binding are absent in this mutant.

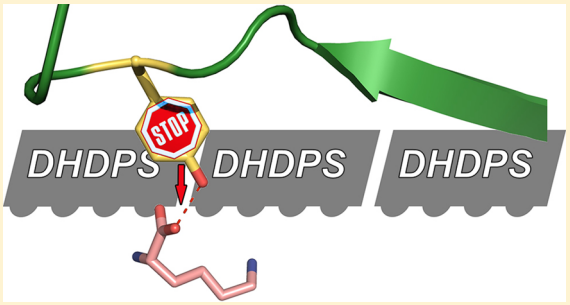

Dihydrodipicolinate synthase (DHDPS) catalyzes the condensation of pyruvate and (*S*)-aspartate-*β*-semialdehyde (ASA) to form (4*S*)-4-hydroxy-2,3,4,5-tetrahydro-(2*S*)-dipicolinic acid (HTPA), which spontaneously dehydrates to dihydrodipicolinic acid in solution (Scheme 1).[1,2] DHDPS controls the first committed step in the *meso*-diaminopimelate pathway for the biosynthesis of L-lysine, which is common to many bacteria and plant species but absent in animals. Lysine and *meso*-diaminopimelate are necessary for bacterial cell wall synthesis and, therefore, the survival of the organism. DHDPS is controlled through allosteric feedback inhibition by lysine, the final product in the diaminopimelate pathway.[2] DHDPS has received considerable attention over the past 15 years as a potential antibiotic target, although no potent inhibitors have been reported to date.[2−5] In plants, lysine is often a limiting nutrient, and plant biotechnologists have expressed keen interest in engineering crops with noninhibitable DHDPS activity.[6,7]

Scheme 1. Reaction Catalyzed by DHDPS

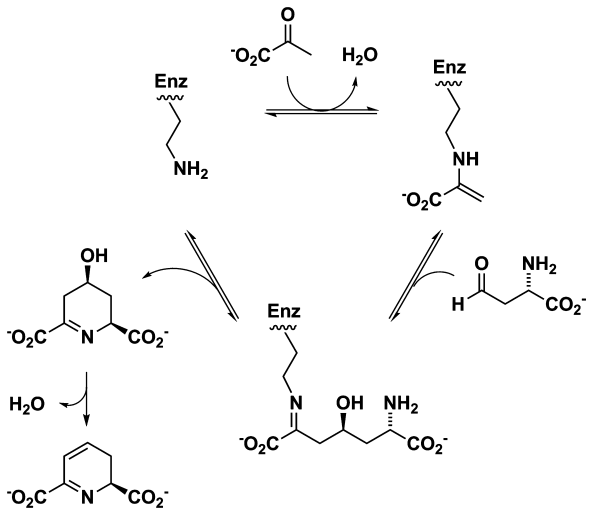

Significant effort has been focused on characterizing the enzymatic mechanism of DHDPS from *Escherichia coli* (*Ec*DHDPS) and other species through mutagenesis,[8−11] crystallography,[8,12−14] nuclear magnetic resonance (NMR),[1,9] and isothermal titration calorimetry.[9,15,16] DHDPS usually exists as a tetramer in solution, best described as a dimer of tight dimers, where the allosteric site of inhibition is formed by the tight dimer interface.[17] DHDPS uses a type I aldolase mechanism characterized by ping-pong kinetics.[1−3,5,9,18] The first step involves the formation of a Schiff base between an active-site lysine residue and pyruvate.[19−21] Binding of ASA results in aldol condensation with the internal enamine, followed by cyclization and release of HTPA (Scheme 1).[5,9] Site-directed mutagenesis studies indicate that general acid/base catalysis is facilitated by a "catalytic triad" consisting of a tyrosine residue adjacent to the active-site lysine, a threonine residue, and another tyrosine that extends into the active site of an adjacent monomer of the oligomeric (usually tetrameric)

Received: September 26, 2014
Revised: October 31, 2014
Published: November 4, 2014

dx.doi.org/10.1021/bi5012157 | *Biochemistry* 2014, 53, 7396−7406

enzyme; in *Ec*DHDPS, these are Tyr133, Thr44, and Tyr107′ (where the primed residue originates from an adjacent monomer).[22] Notably, the last of these residues is adjacent to another tyrosine residue, Tyr106′, which extends into the allosteric site at the dimer interface.[8] This pair of tyrosine residues connecting the active and allosteric sites is highly conserved among lysine-sensitive DHDPS.

The tight dimer interface is required for lysine inhibition across all species.[17] Available crystal structures all show that two lysine molecules bind at this interface in a head-to-head fashion with 2-fold symmetry[8,12−14] and each lysine makes hydrogen bonding interactions with both monomers.[11,22] The carboxyl of each lysine forms hydrogen bonds with the hydroxyl of a tyrosine of the first monomer, while the carboxyl and α-amino groups of the lysine are bound to the second monomer by an asparagine in the "floor" of the allosteric site. The α-amino group is also bound to the second monomer by a glutamic acid residue near the opening of the site. The ε-amino group is coordinated by hydrogen bonds to a histidine and backbone carbonyl oxygens inside the allosteric site. The ε-amino group is capped at the surface by another histidine that forms a π interaction.

Dobson et al. performed a structural comparison of *Ec*DHDPS by superimposing the pyruvate-bound structure [Protein Data Bank (PDB) entry 1YXC] onto a second structure with an empty active site and a lysine bound to the allosteric site (PDB entry 1YXD).[11] The authors observed only minor residue movements between the two protein structures. Together with the NMR observations of Blickling et al.,[1] several mechanisms have been proposed to explain lysine inhibition. In *Ec*DHDPS, it was proposed that inhibition is caused by a perturbation of the proton relay of the catalytic triad, resulting from a small change in the position of Tyr107′.[22] Alternatively (or perhaps additionally), the binding of lysine may disrupt a conserved water channel that connects the active site to the allosteric site, preventing Schiff base formation.[22] L-Lysine may stabilize a less catalytically competent conformer to prevent the binding or reaction of ASA.[16] The observed modes of inhibition suggest that lysine and pyruvate can be bound at the same time, and kinetic studies of cooperativity show that pyruvate actually improves lysine binding.[9,23,24] More recently, the importance of the quarternary structure has been demonstrated.[25] Dimeric variants of DHDPS exhibit reduced catalytic activity, suggesting that the tetrameric structure optimizes enzyme dynamics for catalysis. Griffin et al. probed the sensitivity of the dimer−dimer interface with a series of point mutations[26] and showed that single-point mutations have an effect on both catalysis and tetramerization. The dimer−dimer interface is small and not well conserved across species; however, there is much agreement between the proteins from *E. coli* and *Campylobacter jejuni*. It is not yet clear how lysine binding affects the tetrameric structure or dynamics.

We have recently studied the kinetics of both catalysis and inhibition of DHDPS from *C. jejuni* (*Cj*DHDPS),[23] a human and animal pathogen.[27] Structures of *Cj*DHDPS have been deposited in the PDB by the Center for Structural Genomics of Infectious Diseases (CSGID) in the apo form and with pyruvate covalently bound to the active site (PDB entries 3M5V and 3LER, respectively). *Cj*DHDPS shares 37% identity with *Ec*DHDPS, shares the same fold, and has conserved residues that are required for both substrate and lysine binding. The K_i of lysine is several times higher for *Ec*DHDPS than for *Cj*DHDPS.[23,24] In *Cj*DHDPS, lysine exhibits uncompetitive partial inhibition with respect to pyruvate and mixed partial inhibition with respect to ASA, differing from the reported kinetic model for *Ec*DHDPS.[9,23,24] One outcome of the uncompetitive mechanism of inhibition with respect to pyruvate is that the presence of pyruvate apparently enhances the binding of lysine to the allosteric site.[23] The relatively strong inhibition and distinct kinetic mechanism of inhibition of *Cj*DHDPS by lysine prompted us to investigate whether this enzyme would reveal any further information regarding structural changes induced by inhibitor binding. The structures that we describe in this paper represent the first structures of DHDPS from a bacterial species that contain both lysine and pyruvate bound in their respective sites. These structures provide the first analysis of the cooperative nature of pyruvate and lysine binding. Our analysis indicated a critical role for Tyr110 (the functional analogue of *E. coli* residue Tyr106), and the mutation of Tyr110 to phenylalanine showed both kinetic and structural changes consistent with a critical role for this residue in lysine inhibition.

EXPERIMENTAL PROCEDURES

Cloning and Overexpression. *E. coli* strain XL1-Blue was transformed with a plasmid containing the *dapA* gene (encoding DHDPS, or its mutant, bearing an N-terminal hexahistidine tag) as previously described.[23] The cells were cultured overnight at 310 K in Terrific Broth medium containing 50 μg/mL ampicillin. Overexpression of DHDPS was induced via the addition of isopropyl 1-thio-β-D-thiogalactopyranoside (IPTG) to a concentration of 0.5 mM and incubated for a further 15 h at 288 K. Cells were pelleted at 277 K by centrifugation at 4400*g* for 30 min and stored at 193 K.

Purification. Frozen cell pellets were resuspended in 25 mL of lysis buffer [50 mM HEPES, 500 mM NaCl, 5% glycerol, and 5 mM imidazole (pH 8.0)] with 0.2 mg of DNase and 0.4 mg of lysozyme. Cells were disrupted by sonication (15 s on and 15 s off for 3 min, level 6) using a Virsonic 600 Ultrasonic Cell Disrupter. The supernatant was separated from the cell debris by centrifugation at 27000*g* for 10 min at 277 K. The supernatant was passed through a 0.45 μm filter and loaded onto a 20 mL POROS MC20 histidine affinity column (Applied Biosystems). The column was washed with lysis buffer until the UV absorption of the eluent returned to baseline. DHDPS was eluted from the column by an imidazole gradient from 5 to 500 mM. The purity of collected fractions was assessed by sodium dodecyl sulfate−polyacrylamide gel electrophoresis. Pure fractions of DHDPS were pooled and dialyzed overnight [20 mM HEPES, 250 mM NaCl, 2 mM DTT, and 10% (v/v) glycerol (pH 8.0)] and then concentrated using Sartorius Stedim Vivaspin 20 centrifuge filters. The protein was aliquoted into 50 μL fractions at a concentration of ∼10 mg/mL and flash-frozen in liquid nitrogen before being stored at 193 K.[23]

Crystallization. The commercially available screening kit PEGII Suite (Hampton Research) was selected for its broad overlap of crystallization conditions reported for DHDPS from *C. jejuni* and other species.[8,12−14] Crystallization trials were conducted at 287 K using 96-well sitting drop plates from Hampton Research. Sitting drops were mixed with 1.0 μL of protein solution (∼10 mg/mL) and 1.0 μL of precipitant solution with a 100 μL well of the same precipitant solution. Several positive hits were identified and selected for further optimization using the hanging drop method with 3 μL drops

dx.doi.org/10.1021/bi5012157 | *Biochemistry* 2014, 53, 7396−7406

Table 1. Crystallographic Data for DHDPS Structures[a]

	wt:apo (4R53)	wt:pyr (4LY8)	wt:pyr:lys (4M19)	Y110F:pyr (4MLJ)	Y110F:pyr:lys (4MLR)
growth conditions	0.2 M sodium acetate, 20% PEG4000, 0.1 M TRIS (pH 8.5)	0.25 M sodium acetate, 18% PEG4000, 0.1 M TRIS (pH 8.5)	0.25 M sodium acetate, 20% PEG4000, 0.1 M TRIS (pH 8.5)	0.2 M sodium acetate, 18% PEG4000, 0.1 M TRIS (pH 8.5)	0.15 M sodium acetate, 17% PEG4000, 0.1 M TRIS (pH 8.5)
temperature (K)	100	100	100	100	100
X-ray source	CLS (08BM-01)	CLS (08ID-01)	CLS (08B1-1)	CLS (08ID-01)	CLS (08ID-01)
wavelength (Å)	0.97952	0.9796	0.9798	0.9798	0.9795
distance (mm)	250.00	239.993	289.995	250.00	239.936
space group	$P2_1$	$P2_12_12_1$	$P2_1$	$P2_12_12_1$	$P2_1$
unit cell parameters	a = 77.2 Å, b = 97.6 Å, c = 82.4 Å, $\alpha = \gamma = 90°$, $\beta = 104.47°$	a = 81.3 Å, b = 101.4 Å, c = 148.0 Å	a = 78.6 Å, b = 97.0 Å, c = 79.6 Å, $\beta = 111.5°$	a = 81.1 Å, b = 97.9 Å, c = 149.7 Å	a = 91.0 Å, b = 97.6 Å, c = 131.4 Å, $\beta = 92.1°$
resolution range (Å)	46−2.0 (2.07−2.0)	43.01−1.60 (1.66−1.60)	50−2.0 (2.05−2.0)	41−2.10 (2.17−2.10)	43.45−2.20 (2.28−2.20)
no. of measured reflections	324248	886712	280550	251823	485813
no. of unique reflections	77665	158522	73356	63293	116487
R_{sym} (%)	17.8 (117.7)	14.0 (54.1)	8.1 (51.2)	19.2 (60.8)	16.8 (78.4)
R_{merg} (%)	25.3 (116.0)	12.9 (44.0)	12.99 (56.9)	16.8 (52.6)	14.7 (68.6)
completeness (%)	99.9 (99.9)	98.3 (89.1)	97.6 (80.8)	90.16 (93.15)	99.9 (100)
mean $I/\sigma(I)$	7.95 (1.64)	5.8 (1.5)	17.61 (3.21)	7.16 (2.18)	4.5 (1.4)
Matthews coefficient (Å^3/Da)	2.15	2.24	2.07	2.18	2.14
solvent content (%)	42.87	45.15	40.65	43.7	42.66
no. of molecules in the asymmetric unit	4	4	4	4	8

[a]Numbers in parentheses refer to values for the outer shell.

dx.doi.org/10.1021/bi50121571 | Biochemistry 2014, 53, 7396−7406

Table 2. Refinement Statistics for DHDPS

	apo:DHDPS (4R53)	wt:pyr (4LY8)	wt:pyr:lys (4M19)	Y110F:pyr (4MLJ)	Y110F:pyr:lys (4MLR)
resolution range (Å)	46.03−2.00	43.03−1.70	48.51−1.99	48.6−2.1	43.45−2.20
R_{work}/R_{free} (%)	17.4/21.3	20.9/25.5	15.1/19.2	20.19/24.36	21.9/26.8
no. of amino acid residues	1183	1190	1185	1187	2371
no. of solvent atoms	579	651	533	407	202
no. of ligands	0	4	8	4	16
rmsd					
bond lengths (Å)	0.005	0.006	0.006	0.007	0.003
bond angles (deg)	0.928	1.11	1.02	1.09	0.820
B factor (Å^2)					
DHDPS tetramer	22.4	25.40	25.40	26.40	49.90
pyruvate	–	32.49	23.04	38.70	59.86
lysine	–	–	16.58	–	55.15
Ramachandran plot (%)					
most favored	97.79	97.19	97.16	98	96.88
additionally allowed	2.21	2.13	2.49	2.00	2.90

mixed in a 1:1 ratio over a 500 μL well. The best crystallization conditions for each crystal are reported in Table 1.

Ligand Soaking. The inhibitor L-lysine was introduced into crystallized DHDPS as a component of the cryoprotectant solution (10% ethylene glycol, 30% PEG 400, and 60% precipitant solution with 10 mM lysine for the wild type and 30 mM lysine for Y110F). In the absence of lysine, crystals were stable in the cryoprotectant solution. With lysine present in the cryoprotectant, crystal quality degraded if the crystal was soaked for an extended period. Crystals that maintained diffraction quality were soaked in the aforementioned cryoprotectant solution for 5 min before being flash-cooled in liquid nitrogen.

Removal of Pyruvate from the Active Site. Because the *Cj*DHDPS enzyme is copurified with pyruvate bound in the active site, it was necessary to incubate the enzyme with ASA to obtain the apo form of the enzyme. Prior to crystallization, purified DHDPS was incubated with 10 mM ASA for 30 min. This was followed by dialysis [20 mM HEPES, 250 mM NaCl, and 2 mM DTT (pH 8.0)] to remove excess ASA and dihydrodipicolinic acid.

Data Collection and Refinement. Diffraction experiments were conducted using synchrotron radiation at the Canadian Light Source (CLS) on the 08B1-01 and 08ID-01 beamlines equipped with a MAR CCD 300 area detector. The images were integrated and scaled using either auto-XDS/XSCALE in-house at the CLS or d*Trek.[28,29] Pertinent data collection statistics are listed in Table 1.

Lysine-soaked crystals and apo crystals were found to be of space group $P2_1$, while crystals without lysine were of group $P2_12_12_1$. The structures were determined by molecular replacement with MolRep from the CCP4 suite using the solvent-stripped wild-type structure (PDB entry 3M5V) as the search model.[30] The solution found four monomers organized as a tetramer in the asymmetric unit, with the exception of the Y110F:lys structure that contains two tetramers in the asymmetric unit. Solvent contents determined from Matthews coefficients were consistently between 40 and 45%.[31] Further refinements were made using PHENIX,[32] with manual model correction in COOT.[33] Structure quality was assessed using MolProbity[32] and validation tools in COOT.[33] Final refinement statistics are listed in Table 2.

Ligand Identification. The electron $F_o - F_c$ (3.0σ) difference map from all data sets showed clear positive density within the active site, consistent with the Schiff base formed by Lys166 and pyruvate, with the exception of apo-*Cj*DHDPS. Pyruvate had not been introduced at any time and therefore indicates copurification with the DHDPS enzyme. Molecular replacement and refinement of the ligand-soaked crystals indicated the expected difference density for Lys166-pyruvate Schiff base in the active site, as well as unambiguous positive lysine inhibitor density in the allosteric site of each monomer (Figure 1b).

Site-Directed Mutagenesis. The Y110F mutation was generated using the KAPA HiFi PCR Kit (Kapa Biosystems) according to the manufacturer's recommendations. A mutagenic primer was designed to introduce the required mutation: 5′-GATTTTAAGTGTGGC*G*CCGT**T**TTATAATAAACCTACGCAACAAG-3′, where one mutation introduces phenylalanine (shown in bold) and an additional silent mutation (shown in bold italic) was made to generate a new restriction site, *Nar*I (underlined), for the purpose of screening plasmids isolated from *E. coli* XL1-Blue transformants. Isolated plasmid DNA from selected clones was sequenced by the DNA Technologies Unit of the National Research Council (Saskatoon, SK). For the purpose of kinetic assays, the Y110F protein was expressed, purified, and concentrated to 1.21 mg/mL, as previously described for wt-DHDPS from *C. jejuni*.[23]

Enzyme Kinetics. Pyruvate, L-lysine, and NADH were obtained from Sigma-Aldrich Canada, Ltd. (Oakville, ON), and 2-[4-(2-hydroxyethyl)piperazin-1-yl]ethanesulfonic acid (HEPES) was purchased from BDH (Mississauga, ON). (*S*)-Aspartate-β-semialdehyde was synthesized according to the reported procedure.[34] The concentration of each newly prepared work solution of ASA was determined using the DHDPS−DHDPR-coupled kinetic assay, in the presence of excess NADH.[23,35] The activity of the Y110F mutant was measured using a coupled assay in 100 mM HEPES buffer at pH 8.0 and 298 K as previously described for the wild-type enzyme.[23,35] The obtained kinetic data were fit to the rate equation describing a ping-pong kinetic mechanism (eq 1) using SigmaPlot 11.0 (Systat Software, San Jose, CA):

$$\nu = V_{max}AB/[K_{M(B)}A + K_{M(A)}B + AB] \quad (1)$$

where V_{max} is the maximal velocity, $K_{M(A)}$ and $K_{M(B)}$ are the Michaelis−Menten constants for two substrates, A and B are the concentrations of the substrates, and ν is the initial velocity.

dx.doi.org/10.1021/bi5012157 | *Biochemistry* 2014, 53, 7396−7406

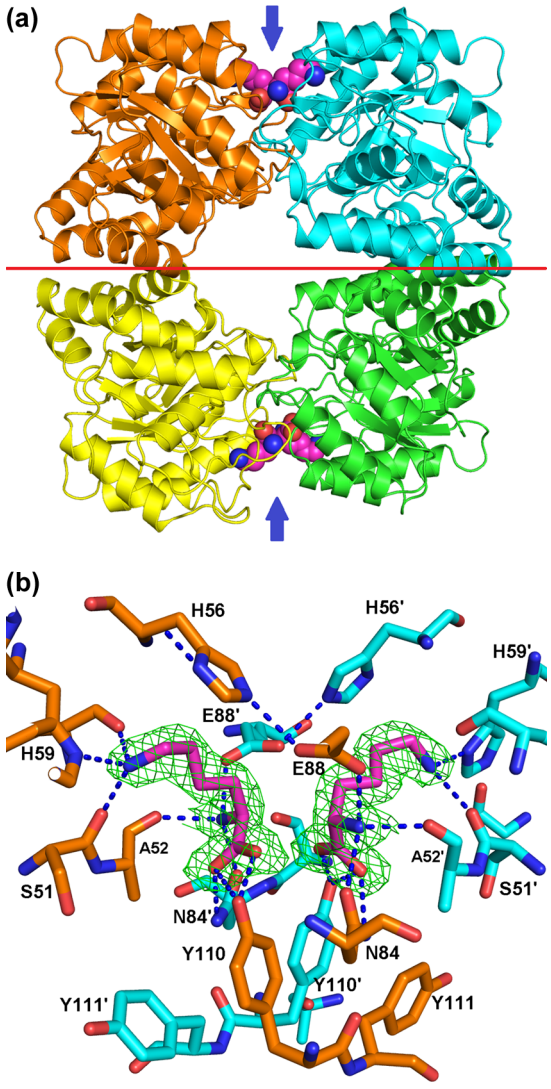

Figure 1. *Cj*DHDPS bound to L-lysine. Panel a shows the DHDPS tetramer (PDB entry 4M19). The blue arrows indicate the allosteric binding site at the tight dimer interface. The red line denotes the weak dimer−dimer interface. Bound L-lysine is depicted as spheres. Panel b shows the omit map for lysine bound to the allosteric site of wt DHDPS. The omit map is depicted as green mesh with no lysine present, contoured at 3σ, with monomer A colored orange and monomer B (primed residues) colored blue. Newly formed hydrogen bonds are shown as blue dashed lines. A single lysine molecule forms hydrogen bonds with residues from both monomers, and the second lysine binds with 2-fold symmetry.

In this case, *A* refers to the first substrate, pyruvate, and *B* refers to ASA.

The inhibition of DHDPS by lysine was examined using the conditions described above over a lysine concentration range of 0−80 mM at a saturating concentration of pyruvate (3.70 mM) and a near-K_M concentration of ASA (0.12 mM).

RESULTS AND DISCUSSION

Structure of *Cj*DHDPS Complexed with Lysine. All *Cj*DHDPS crystals contained pyruvate bound as a Schiff base to the active-site lysine (Lys166), indicating that pyruvate is copurified with the enzyme, and this structure likely represents the resting state of the enzyme. The apo-*Cj*DHDPS structure (PDB entry 4R53) was obtained by incubation with 10 mM ASA for 30 min followed by dialysis prior to crystallization. We obtained crystals of the *Cj*DHDPS:pyr:lys complex (PDB entry 4M19) by soaking the crystals in a cryoprotectant, consisting of a mix of 10% ethylene glycol, 30% PEG 400, and 60% precipitant solution, including 10 or 30 mM lysine, for 5 min. Extended soaking times resulted in decreased diffraction quality. Crystals soaked in this manner consistently diffracted to better than 2.5 Å resolution. Our best crystals diffracted to 1.6 Å resolution, and the structure was determined by molecular replacement (Table 1). The structure of the *Cj*DHDPS:pyr complex (PDB entry 4LY8) was refined with a resolution of 1.6 Å and is similar to the previously reported structures (PDB entry 3LER) with a Cα rmsd of 0.29 Å. Apo-*Cj*DHDPS (PDB entry 4R53) was refined at a resolution of 2.0 Å, and its structure is similar to the previously reported structure of PDB entry 3M5V with a Cα rmsd of 0.18 Å (Table 2). The structure of the *Cj*DHDPS:pyr:lys complex (PDB entry 4M19) was determined to 2.0 Å, and each allosteric cleft contains two lysine molecules bound in a "head-to-head" orientation, that is, with α-carbons in the proximity of each other, in the allosteric site (Figure 1).

As observed in other DHDPS structures, the allosteric binding site exists at the tight dimer interface, and the binding site for a single lysine molecule is comprised of residues from both monomers. Two lysine molecules bind in a head-to-head fashion with 2-fold symmetry (Figure 1),[8,12−14] and each lysine makes hydrogen bond interactions with both monomers. A comparison of the *Cj*DHDPS:pyr:lys (PDB entry 4M19) structure to the *Cj*DHDPS:pyr (PDB entry 4LY8) structure revealed several side chain movements to accommodate lysine in the allosteric site (Figure 2). For a lysine molecule bound to the allosteric site of monomer A, the carboxyl of lysine is hydrogen bonded to Tyr110 in monomer A. The α-amino group is hydrogen bonded to Ala52 from monomer A, and

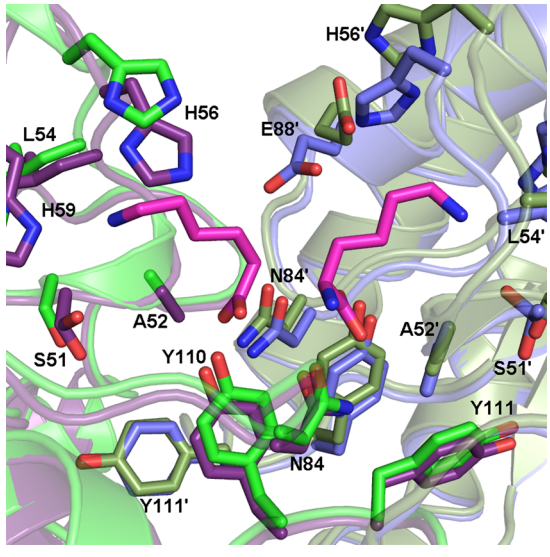

Figure 2. Superposition of *Cj*DHDPS:pyr:lys and wt:pyr complexes. The *Cj*DHDPS:pyr:lys structure (PDB entry 4M19) is colored green, and the *Cj*DHDPS:pyr structure (PDB entry 4LY8) is colored purple (different shades indicate each monomer). There is some disorder introduced at the side chain of S51; therefore, two possible conformations are represented. The superposition highlights that many residues make minor shifts to accommodate the binding of lysine (colored magenta).

dx.doi.org/10.1021/bi5012157 | *Biochemistry* 2014, 53, 7396−7406

Asn84/Glu88 from monomer B. The ε-amino group forms hydrogen bonds with His59, and the backbone carbonyls of Ser51 and Leu54 of monomer A. The 2-fold symmetry of *Cj*DHDPS results in the same interactions for the lysine bound to monomer B. This is consistent with lysine binding patterns reported from homologous species.[11]

There are only minor changes seen between the active sites of *Cj*DHDPS:pyr (PDB entry 4LY8) and *Cj*DHDPS:pyr:lys (PDB entry 4M19) complexes upon binding of lysine to the allosteric site. Small but measurable changes in the distance between pairs of residues are seen for the following pairs: Y137−T47 (from 3.4 to 2.9 Å), Y137−Y111′ (from 4.7 to 4.2 Å), and C1 of the pyruvyl Schiff base and the carbonyl of I207 and G190 (from 3.8 to 4.5 Å and from 4.7 to 3.7 Å, respectively).

Lysine Induces Domain Scale Conformational Changes in DHDPS. While the *Cj*DHDPS:pyr:lys (PDB entry 4M19) structure was very similar to the *Cj*DHDPS:pyr (PDB entry 4LY8) structure, crystal quality was observed to degrade when lysine was included in the cryoprotectant but remained stable when lysine was absent from the cryoprotectant. These observations suggest lysine may induce some conformational changes. Close examination of the superimposed structures revealed notable misalignment and contracted helices. We used DynDom to reveal a subtle concerted domain movement.[36−38] DynDom identifies domains on the basis of vector movements and determines the average vector movements based on a reference structure. Each identified domain is matched to the equivalent section in the unbound protein using a root-mean-square difference (rmsd) of Cα atoms. Our analysis of the *Cj*DHDPS:pyr:lys (PDB entry 4M19) structure demonstrated that there is a concerted domain movement caused by the binding of lysine. The fixed domain is comprised of the N- and C-termini, residues 1−80 and 188−298, respectively. The moving domain consists of residues 104−184. At the interface of moving and fixed domains are residues that lie on or very near the bending axis. Identified domains are highlighted on a single monomer and on the tight dimer formation in Figure 3.

The bending axis is defined by a closure value of 0.798, which represents the amount of hinging as opposed to twisting. A value of >0.5 indicates a predominantly hinged motion rather than a screw axis.[36−38] The moving domain shifts 3.8° on its hinge axis, resulting in a maximal Cα displacement of 2.0 Å at Thr115. Domain movements indicate that half of each monomer rotates toward the allosteric site (Figure 3). The domain shifts are consistent with the closing of the helices around the lysine in the allosteric site.

Implications of Domain Movement for Inhibition. Our principal interest is in understanding the effect of inhibitor binding and associated domain movements on the catalytic site and how this results in loss of DHDPS activity. In the absence of other major changes, the observed domain movement may imply altered protein dynamics such that occupation of the allosteric site restricts the normal movement of domains necessary for catalytic turnover. Studies of DHDPS from other sources have suggested that protein dynamics may be an important aspect of catalysis.[25,39−41] At the heart of the moving domain is a pair of tyrosine residues, Y110 and Y111. Y110 is one of only three residues (Y110, N84, and E88) in the moving domain that makes a direct hydrogen bond to the inhibitor lysine. The neighboring residue Y111 interdigitates across the tight dimer interface to complete the catalytic triad (Y137, T47, and Y111) in the active site of the neighboring monomer (Figure 4). Therefore, Y110/Y111 was identified as a possible link between the allosteric site and the active site.

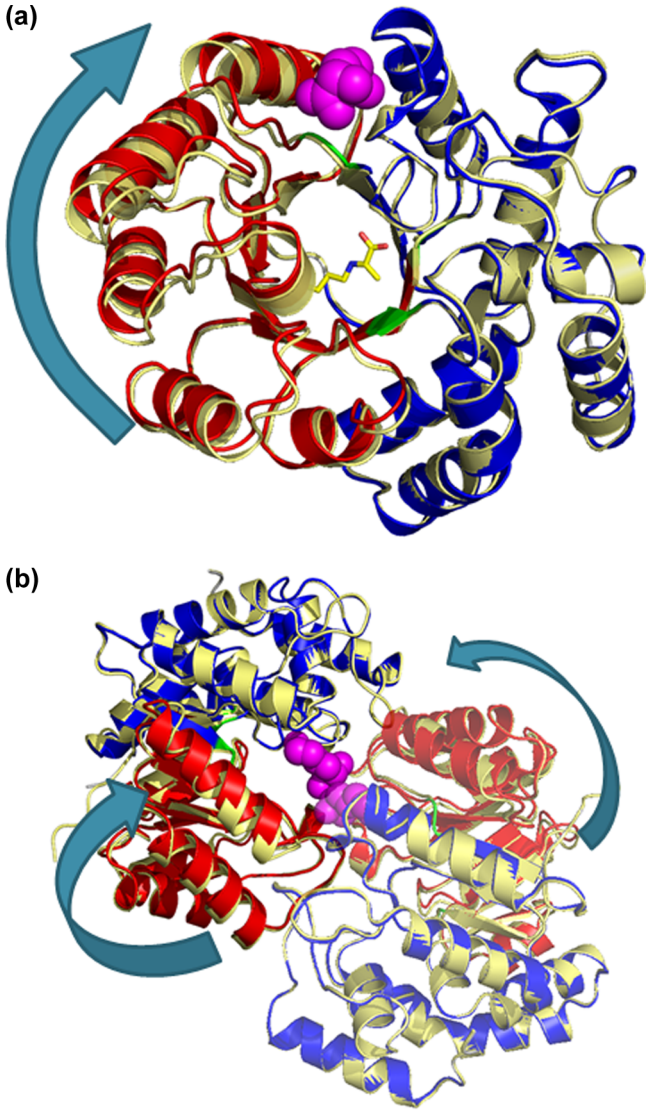

Figure 3. Domain movements in wild-type *Cj*DHDPS. (a) Highlighted domains in a superposition of *Cj*DHDPS:pyr:lys and *Cj*DHDPS:pyr structures. In the *Cj*DHDPS:pyr:lys structure (PDB entry 4M19), the fixed domain is colored blue, the moving domain is colored red, and hinging residues are colored green. The *Cj*DHDPS:pyr structure (PDB entry 4LY8) is colored yellow. L-Lysine bound to the allosteric site (magenta) belongs to the blue and red structure. The blue arrow shows the monomeric hinging action where the moving (red) domain shifts to close the allosteric site. (b) Interplay of monomers at the tight dimer interface. Identical domain movements in each monomer close the allosteric site around two lysine molecules.

The moving domain includes significant contacts in the region of both the tight and weak dimer interface. The tetrameric structure is critical for natural activity and inhibition.[25] At the tight dimer interface, it is well documented that two lysines bind cooperatively in each allosteric cleft,[8,12−14] and we have shown that lysine binding in *Cj*DHDPS is cooperative across the weak dimer interface, as well, as indicated by Hill coefficients of >2.[23] The moving domain extends from the allosteric site into the weak dimer interface. At

dx.doi.org/10.1021/bi5012157 | *Biochemistry* 2014, 53, 7396−7406

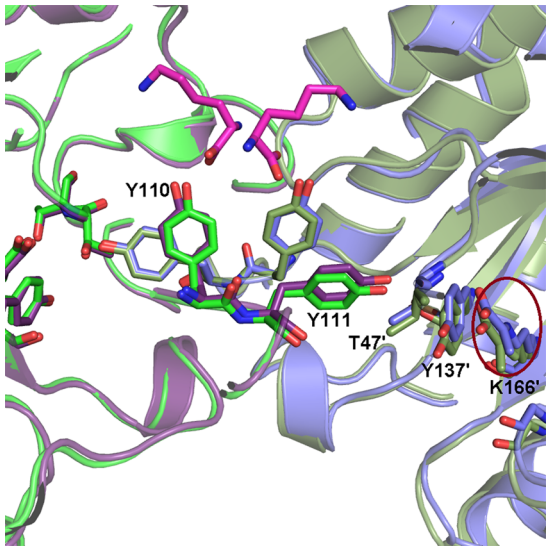

Figure 4. Aromatic pair Y110/Y111 that links the allosteric site and the active site. The *Cj*DHDPS:pyr:lys (PDB entry 4M19) structure is colored purple with lysine colored magenta, and the *Cj*DHDPS:pyr (PDB entry 4LY8) structure is colored green (different shades indicate each monomer). The K166-pyruvate enamine is highlighted with a red circle. The Y110/Y111 aromatic pair links the carboxyl of the inhibitor lysine to the catalytic triad of the active site.

this interface, we find several cross-dimer interactions that have shifted in the DHDPS:pyr:lys (PDB entry 4M19) structure. Rearrangements include the breaking of hydrogen bonds between H181′ and N242 (Figure 5a), N201′ and D238, N201′(CO) and K234, and S200′(CO) and Y196 (Figure 5b), and the alteration of a hydrophobic pocket [I172, V176, I194, I172′, and I194′ (Figure 5c)] by the shift of the side chains by 1.5−2.0 Å. These residues may be implicated in the weak dimer cooperativity signal.

Ligand Binding Affects the Volume of the Active and Allosteric Sites. The observed domain movements appear to be coupled with closure of the allosteric site upon lysine binding. This observation leads us to measure the volume of the active site and allosteric site in each of our wild-type crystal structures. Using CASTp,[42,43] we compared the solvent accessible volume of active sites and allosteric sites in apo-*Cj*DHDPS, *Cj*DHDPS:pyr, and *Cj*DHDPS:pyr:lys structures. These comparisons reveal that the binding of each ligand changes the volume of both the active site and the allosteric site (Table 3). The binding of pyruvate to apo-*Cj*DHDPS (PDB entry 4R53) decreases the active-site volume by 44%. Additionally, the allosteric-site volume is reduced by 16%. The reduction in allosteric-site volume could improve the affinity of the allosteric site for lysine by both improving the orientation of binding groups and providing an entropic effect of limiting lysine conformations.

Binding of lysine reduces the volume of the allosteric site by a further 44%. At the active site, the volume increases by 30% upon lysine binding. An image representative of the change in allosteric-site volume from apo-*Cj*DHDPS to *Cj*DHDPS:pyr:lys was generated using Hollow[44] and is shown in Figure 6; overall, the cavity is observed to shrink in all dimensions as the surrounding helices and residues move toward the center of the cavity. This effect may play a crucial role in the inhibition of the enzyme, likely by reducing the affinity of the active site for ASA.

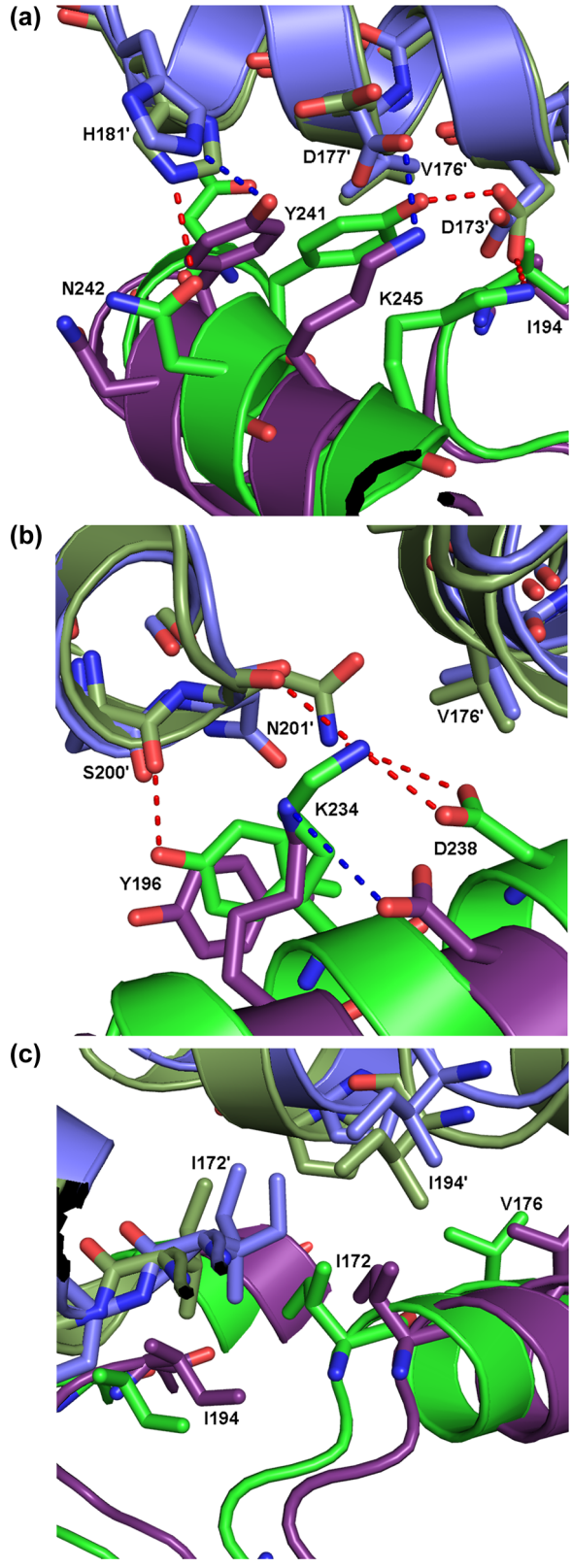

Figure 5. Changes at the dimer−dimer interface. The *Cj*DHDPS:pyr:lys (PDB entry 4M19) structure is colored green and the *Cj*DHDPS:pyr (PDB entry 4LY8) structure purple (different shades indicate each monomer). The dashed blue line denotes hydrogen bonds that are present only in the DHDPS:pyr:lys structure, while the red dashed line denotes hydrogen bonds present only in the DHDPS:pyr structure. Panel a depicts the breaking of a hydrogen bond between H181′ and N242 and between D173′ and Y241, and

dx.doi.org/10.1021/bi5012157 | *Biochemistry* 2014, 53, 7396−7406

Figure 5. continued

the formation of hydrogen bonds between H181′ and Y241, and between D177′ and K245. Panel b shows the disruption of hydrogen bonds between N201′ and D238, N201′(CO) and K234, and S200′(CO) and Y196; residues K234 and D238 move together to retain their hydrogen bond. Panel c shows the rearrangement of a hydrophobic pocket formed by I172, V176, I194, I172′, and I194′. These changes may contribute to the cooperativity observed among four lysine binding sites.

Table 3. Effect of Ligand Binding on the Active-Site and Allosteric-Site Volumes of *Cj*DHDPS Protein Forms

	apo (4R53)	wt:pyr (4LY8)	wt:pyr:lys (4M19)	Y110F:pyr (4MLJ)	Y110F:pyr:lys (4MLR)
active-site volume[a] (Å^3)	36	20	26	22	20
allosteric-site volume[a] (Å^3)	494	417	239	446	332

[a]Solvent accessible volumes calculated using CASTp[42,43] as described in the text, and excluding lysine from the model.

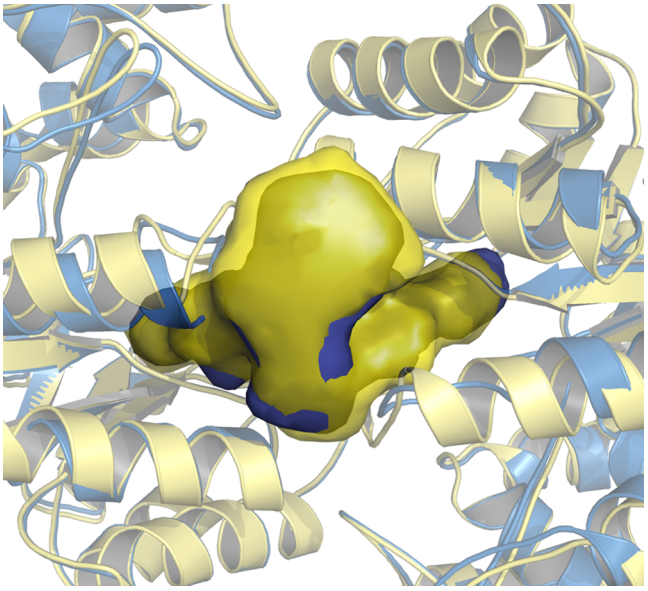

Figure 6. Change in the volume of the allosteric site. The calculated allosteric cavity is rendered with Hollow[44] for apo-*Cj*DHDPS in transparent yellow (larger) and *Cj*DHDPS:pyr:lys in blue (smaller). The structure of apo-*Cj*DHDPS is colored yellow and that of *Cj*DHDPS:pyr:lys blue. The allosteric cavity shrinks in all dimensions as the surrounding helices and side chains move toward the center of the cavity.

Significance of Y110. In wt-*Cj*DHDPS, we identified the Y110/Y111 aromatic pair as a possible link between the allosteric site and the active site. Y110 forms a hydrogen bond with the carboxyl of the lysine inhibitor; its neighbor Y111 completes the catalytic triad of the opposite monomer. Furthermore, Y110 is one of only three residues in the moving domain that makes hydrogen bonds to the inhibitor lysine. It therefore seems likely that Y110 plays a role in allosteric signal transduction. To probe the importance of the hydrogen bond formed by Tyr110, we generated the site-directed mutant Y110F.

Kinetic data were obtained for Y110F in the presence of varying concentrations of pyruvate (0.15−3.70 mM) and ASA (0.073−2.55 mM), and the resulting rates were fit to eq 1 describing a ping-pong kinetic mechanism as described previously.[23] The mutant apparently operates by the same kinetic mechanism as wt-*Cj*DHDPS and shows only minor differences in the values of the Michaelis constants, as shown in Table 4. The value of k_{cat}, however, is reduced ∼2-fold relative to that of wt-*Cj*DHDPS. The importance of the side chain of Y110 to catalysis is not obvious but likely derives from some effect on the adjacent Y111 (which completes the catalytic triad) or on the nearby secondary and tertiary structure elements of the enzyme.

The Y110F mutation dramatically affects the ability of the enzyme to be inhibited by lysine. The removal of the hydroxyl group results in an estimated L-lysine IC_{50} of ∼40 mM, an increase of 3 orders of magnitude (Figure 7). Our crystal

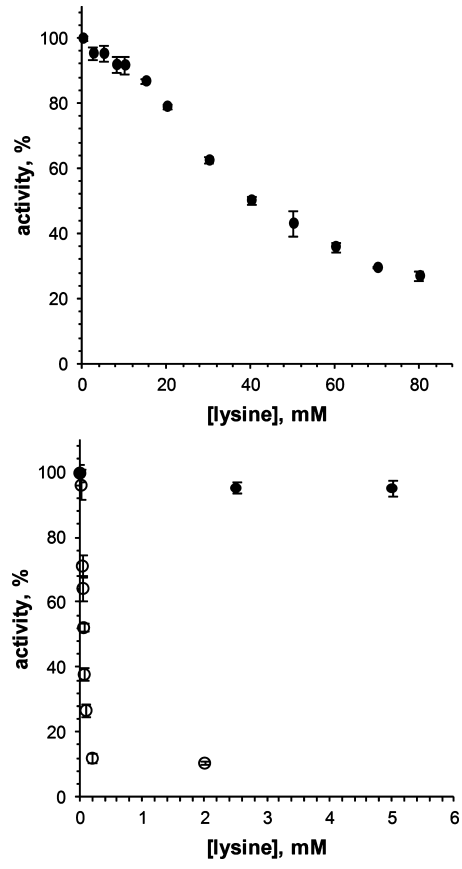

Figure 7. Lysine inhibition curve for Y110F (top) (0.12 mM ASA and 3.70 mM pyruvate). Comparison of lysine inhibition for Y110F (●) and the wild type (○) (bottom) (0.16 mM ASA and 3.50 mM pyruvate).

Table 4. Kinetic Constants for Y110F in Comparison with Those of wt-*Cj*DHDPS

	$K_{M(pyr)}$ (mM)	$K_{M(ASA)}$ (mM)	k_{cat} (s^{-1})	$k_{cat}/K_{M(pyr)}$ (M^{-1} s^{-1})	$k_{cat}/K_{M(ASA)}$ (M^{-1} s^{-1})
Y110F	0.19 ± 0.01	0.12 ± 0.01	33 ± 1	(1.8 ± 0.1) × 10^5	(2.7 ± 0.1) × 10^5
wt-*Cj*DHDPS[23]	0.35 ± 0.02	0.16 ± 0.01	76 ± 1	(2.2 ± 0.1) × 10^5	(4.8 ± 0.3) × 10^5

dx.doi.org/10.1021/bi5012157 | *Biochemistry* 2014, 53, 7396−7406

structure suggests that only one of nine hydrogen bonds formed by the binding of each inhibitor molecule is disrupted by the mutation; only the hydrogen bond between Y110 and the lysine carboxyl is lost, while all other hydrogen bonds remain intact. The effect on inhibition is thus surprisingly strong, suggesting that this particular hydrogen bond is a key contributor to inhibitory signal transduction (Figure 8).

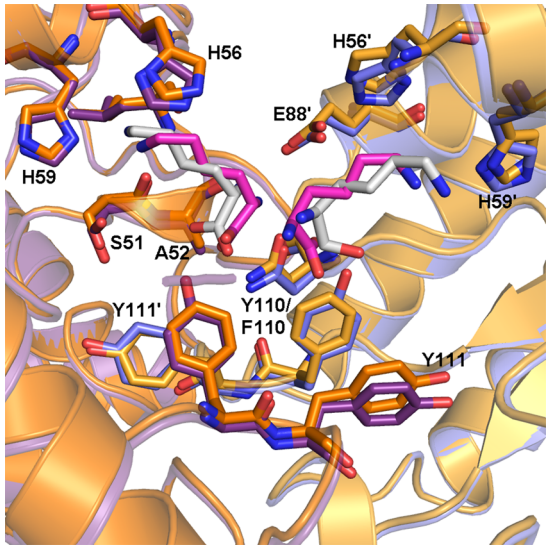

Figure 8. Superposition of Y110F:pyr:lys and *Cj*DHDPS:pyr:lys structures. The *Cj*DHDPS:pyr:lys (PDB entry 4M19) structure is colored purple and the Y110F:pyr:lys (PDB entry 4MLR) structure orange (different shades indicate each monomer). The lysine colored magenta is from the wild-type structure, while the lysines colored gray are from the Y110F structure. The Y110F mutation eliminates only one of nine hydrogen bonds in the allosteric site, resulting in drastically reduced lysine sensitivity.

The Y110F:pyr:lys Structure Resembles the wt-*Cj*DHDPS:pyr Structure. Crystal structures of Y110F were obtained both with and without lysine bound to the allosteric site. Crystallization conditions and pertinent diffraction data can be found in Table 1. Cryoprotectant conditions were the same as for wt-*Cj*DHDPS, with the exception that 30 mM lysine was required to show adequate density in the determined structure.

As described above, each structure was found to contain pyruvate, and with the exception of the missing hydrogen bond at the Phe110 position, lysine adopts the same conformation and makes the same interactions as seen in the wt-*Cj*DHDPS:pyr:lys (PDB entry 4M19) (abbreviated as wt:pyr:lys) structure. Comparison of the Y110F:pyr (PDB entry 4MLJ) structure with the wt:pyr (PDB entry 4LY8) structure shows that they are nearly identical (Cα rmsd of 0.25 Å).

As in the *Cj*DHDPS:pyr:lys (PDB entry 4M19) structure, lysine was clearly seen in the initial $F_o - F_c$ electron density map and is bound in the allosteric site in a head-to-head orientation in the Y110F:pyr:lys (PDB entry 4MLR) structure. All side chain positions and hydrogen bonding networks observed in the *Cj*DHDPS:pyr:lys (PDB entry 4M19) structure are preserved in the Y110F:pyr:lys (PDB entry 4MLR) structure with the exception of the missing Tyr hydroxyl group.

Phe110 is unable to form a hydrogen bond with lysine, and the structure displays few of the shifts associated with the *Cj*DHDPS:pyr:lys (PDB entry 4M19) structure. Although the helices flanking the allosteric site shift when lysine is bound in Y110F, the changes noted for wt-*Cj*DHDPS at the weak dimer interface are missing in the Y110F:pyr:lys (PDB entry 4MLR) structure. Additionally, the domain scale movements noted by DynDom for the *Cj*DHDPS:pyr:lys (PDB entry 4M19) structure are absent in the Y110F:pyr:lys (PDB entry 4MLJ) structure. Therefore, we can conclude that the Y110F:pyr:lys (PDB entry 4MLR) structure is more similar to the structure of the catalytically active *Cj*DHDPS:pyr (PDB entry 4LY8) than to the *Cj*DHDPS:pyr:lys (PDB entry 4M19) structure. Finally, the changes to solvent accessible volume are significantly smaller upon lysine binding in Y110F than in wt-*Cj*DHDPS. The volume of the allosteric site of the Y110F:pyr:lys (PDB entry 4MLR) complex is reduced by only 26% from 445.9 to 331.7 Å^3 (compared to 43% in the wild-type enzyme), and the active-site volume decreases by only 6% from 21.6 to 20.4 Å^3 (compared to a 22% increase) (Table 3).

It is remarkable that all structural changes associated with lysine binding in wt-*Cj*DHDPS have been significantly reduced or eliminated with the loss of a single hydrogen bond in the allosteric site. The kinetic data indicate that Y110 is important for lysine inhibition, while the crystal structures clearly demonstrate that lysine binds but has muted structural effects on the enzyme. Therefore, the hydrogen bond between the inhibitor lysine and Tyr110 is critically important in the effective allosteric signal transduction.

CONCLUSIONS

The high-resolution structures of *Cj*DHDPS and its Y110F mutant have provided new and important insight into the mechanics of allosteric inhibition by L-lysine. Binding of lysine induces domain movement in the wild-type enzyme not previously observed, suggesting that the hydrogen bond network created by the inhibitor molecules between subunits tethers the domain in place, preventing relaxation to a catalytically active conformation. This concerted domain movement has relatively little effect on the observed positions of the active-site residues relative to the lysine-free structure. The moving domains of individual monomers meet at the weak dimer interface, and a rearrangement of cross-monomer interactions takes place. This may provide an explanation of inhibitor cooperativity across the weak dimer interface.

The Y110/Y111 residue pair is identified as a potential link between the allosteric site and the active site. Mutation of Y110 to phenylalanine drastically reduces the inhibitory effect of lysine, although the crystal structure indicates that lysine does bind in the mutated allosteric site. Furthermore, the domain movement observed in wt-*Cj*DHDPS is not observed in the Y110F structure. Therefore, the observed domain movement may be necessary for enzyme inhibition. One explanation is that domain movement in wt-*Cj*DHDPS restricts the dynamics necessary for catalysis. These results clearly identify Y110 as one of the triggers for inhibition.

When lysine binds to DHDPS, only minor residue movements are observed in the allosteric site. However, analysis of cavity volumes indicates a series of volume contractions and expansions caused by the binding of either pyruvate or lysine. Pyruvate reduces the volume of both the active site and allosteric site, while binding of lysine reduces the volume at the allosteric site and increases the volume at the active site. In the Y110F mutant, these volume changes are muted. The changes in volume may explain the cooperativity

dx.doi.org/10.1021/bi5012157 | *Biochemistry* 2014, 53, 7396−7406

observed between pyruvate and lysine binding and provide a possible mechanism for the inhibition of ASA binding or reacting.

AUTHOR INFORMATION

Corresponding Authors

*E-mail: dave.palmer@usask.ca. Phone: (306) 966-4662. Fax: (306) 966-4730.

*E-mail: david.sanders@usask.ca. Phone: (306) 966-6788. Fax: (306) 966-4730.

Funding

This work has been supported by NSERC Discovery grants to D.A.R.S. and D.R.J.P. C.J.T.C. and Y.V.S. were both recipients of NSERC PGS awards.

Notes

The authors declare no competing financial interest.

ACKNOWLEDGMENTS

We thank Dr. Janet Hill and Dr. Bonnie Chaban (Department of Veterinary Microbiology, Western College of Veterinary Medicine, University of Saskatchewan) for providing *C. jejuni* genomic DNA, all the CMCF beamline staff at the Canadian Light Source, and especially Dr. Karin van Straaten and Dr. Sean Dalrymple (Department of Chemistry, University of Saskatchewan) for their tutelage and guidance. The structural studies described in this paper were performed at the CLS, which is supported by NSERC, the National Research Council of Canada, the Canadian Institutes of Health Research, the Province of Saskatchewan, Western Economic Diversification Canada, and the University of Saskatchewan.

ABBREVIATIONS

DHDPS, dihydrodipicolinate synthase; *Cj*DHDPS, *C. jejuni* dihydrodipicolinate synthase; *Ec*DHDPS, *E. coli* dihydrodipicolinate synthase; lys, lysine; pyr, pyruvate; wt, wild-type; ASA, (*S*)-aspartate-β-semialdehyde; rmsd, root-mean-square deviation.

REFERENCES

(1) Blickling, S., Renner, C., Laber, B., Pohlenz, H. D., Holak, T. A., and Huber, R. (1997) Reaction mechanism of *Escherichia coli* dihydrodipicolinate synthase investigated by X-ray crystallography and NMR spectroscopy. *Biochemistry 36*, 24−33.

(2) Hutton, C. A., Perugini, M. A., and Gerrard, J. A. (2007) Inhibition of lysine biosynthesis: An evolving antibiotic strategy. *Mol. BioSyst. 3*, 458−465.

(3) Born, T. L., and Blanchard, J. S. (1999) Structure/function studies on enzymes in the diaminopimelate pathway of bacterial cell wall biosynthesis. *Curr. Opin. Chem. Biol. 3*, 607−613.

(4) Cox, R. J., Sutherland, A., and Vederas, J. C. (2000) Bacterial diaminopimelate metabolism as a target for antibiotic design. *Bioorg. Med. Chem. 8*, 843−871.

(5) Hutton, C. A., Southwood, T. J., and Turner, J. J. (2003) Inhibitors of lysine biosynthesis as antibacterial agents. *Mini-Rev. Med. Chem. 3*, 115−127.

(6) Falco, S. C., Guida, T., Locke, M., Mauvais, J., Sanders, C., Ward, R. T., and Webber, P. (1995) Transgenic canola and soybean seeds with increased lysine. *Nat. Biotechnol. 13*, 577−582.

(7) Varisi, V. A., Medici, L. O., van der Meer, I., Lea, P. J., and Azevedo, R. A. (2007) Dihydrodipicolinate synthase in opaque and floury maize mutants. *Plant Sci. 173*, 458−467.

(8) Dobson, R. C. J., Valegard, K., and Gerrard, J. A. (2004) The crystal structure of three site-directed mutants of *Escherichia coli* dihydrodipicolinate synthase: Further evidence for a catalytic triad. *J. Mol. Biol. 338*, 329−339.

(9) Soares da Costa, T. P., Muscroft-Taylor, A. C., Dobson, R. C. J., Devenish, S. R. A., Jameson, G. B., and Gerrard, J. A. (2010) How essential is the 'essential' active-site lysine in dihydrodipicolinate synthase? *Biochimie 92*, 837−845.

(10) Dobson, R. C. J., Perugini, M. A., Jameson, G. B., and Gerrard, J. A. (2009) Specificity versus catalytic potency: The role of threonine 44 in *Escherichia coli* dihydrodipicolinate synthase mediated catalysis. *Biochimie 91*, 1036−1044.

(11) Dobson, R. C. J., Devenish, S. R. A., Turner, L. A., Clifford, V. R., Pearce, F. G., Jameson, G. B., and Gerrard, J. A. (2005) Role of arginine 138 in the catalysis and regulation of *Escherichia coli* dihydrodipicolinate synthase. *Biochemistry 44*, 13007−13013.

(12) Devenish, S. R. A., Gerrard, J. A., Jameson, G. B., and Dobson, R. C. J. (2008) The high-resolution structure of dihydrodipicolinate synthase from *Escherichia coli* bound to its first substrate, pyruvate. *Acta Crystallogr. F64*, 1092−1095.

(13) Dobson, R. C. J., Griffin, M. D. W., Devenish, S. R. A., Pearce, F. G., Hutton, C. A., Gerrard, J. A., Jameson, G. B., and Perugini, M. A. (2008) Conserved main-chain peptide distortions: A proposed role for Ile203 in catalysis by dihydrodipicolinate synthase. *Protein Sci. 17*, 2080−2090.

(14) Kefala, G., Evans, G. L., Griffin, M. D. W., Devenish, S. R. A., Pearce, F. G., Perugini, M. A., Gerrard, J. A., Weiss, M. S., and Dobson, R. C. J. (2008) Crystal structure and kinetic study of dihydrodipicolinate synthase from *Mycobacterium tuberculosis*. *Biochem. J. 411*, 351−360.

(15) Muscroft-Taylor, A. C., Soares da Costa, T. P., and Gerrard, J. A. (2010) New insights into the mechanism of dihydrodipicolinate synthase using isothermal titration calorimetry. *Biochimie 92*, 254−262.

(16) Phenix, C. P., and Palmer, D. R. J. (2008) Isothermal titration microcalorimetry reveals the cooperative and noncompetitive nature of inhibition of *Sinorhizobium meliloti* L5-30 dihydrodipicolinate synthase by (S)-lysine. *Biochemistry 47*, 7779−7781.

(17) Muscroft-Taylor, A. C., Catchpole, R. J., Dobson, R. C. J., Pearce, F. G., Perugini, M. A., and Gerrard, J. A. (2010) Disruption of quaternary structure in *Escherichia coli* dihydrodipicolinate synthase (DHDPS) generates a functional monomer that is no longer inhibited by lysine. *Arch. Biochem. Biophys. 503*, 202−206.

(18) Karsten, W. E. (1997) Dihydrodipicolinate synthase from *Escherichia coli*: pH dependent changes in the kinetic mechanism and kinetic mechanism of allosteric inhibition by L-lysine. *Biochemistry 36*, 1730−1739.

(19) Borthwick, E. B., Connell, S. J., Tudor, D. W., Robins, D. J., Shneier, A., Abell, C., and Coggins, J. R. (1995) *Escherichia coli* dihydrodipicolinate synthase: Characterization of the imine intermediate and the product of bromopyruvate treatment by electrospray mass-spectrometry. *Biochem. J. 305*, 521−524.

(20) Laber, B., Gomisruth, F. X., Romao, M. J., and Huber, R. (1992) *Escherichia coli* dihydrodipicolinate synthase: Identification of the active-site and crystallization. *Biochem. J. 288*, 691−695.

(21) Shedlarski, J. G., and Gilvarg, C. (1970) The pyruvate-aspartic semialdehyde condensing enzyme of *Escherichia coli*. *J. Biol. Chem. 245*, 1362−1373.

(22) Dobson, R. C., Griffin, M. D., Jameson, G. B., and Gerrard, J. A. (2005) The crystal structures of native and (S)-lysine-bound dihydrodipicolinate synthase from *Escherichia coli* with improved resolution show new features of biological significance. *Acta Crystallogr. D61*, 1116−1124.

(23) Skovpen, Y. V., and Palmer, D. R. J. (2013) Dihydrodipicolinate synthase from *Campylobacter jejuni*: Kinetic mechanism of cooperative allosteric inhibition and inhibitor-induced substrate cooperativity. *Biochemistry 52*, 5454−5462.

(24) Dobson, R. C. J., Griffin, M. D. W., Roberts, S. J., and Gerrard, J. A. (2004) Dihydrodipicolinate synthase (DHDPS) from *Escherichia coli* displays partial mixed inhibition with respect to its first substrate, pyruvate. *Biochimie 86*, 311−315.

(25) Griffin, M. D. W., Dobson, R. C. J., Pearce, F. G., Antonio, L., Whitten, A. E., Liew, C. K., Mackay, J. P., Trewhella, J., Jameson, G. B., Perugini, M. A., and Gerrard, J. A. (2008) Evolution of quaternary structure in a homotetrameric enzyme. *J. Mol. Biol. 380*, 691−703.
(26) Griffin, M. D. W., Dobson, R. C. J., Gerrard, J. A., and Perugini, M. A. (2010) Exploring the dihydrodipicolinate synthase tetramer: How resilient is the dimer-dimer interface? *Arch. Biochem. Biophys. 494*, 58−63.
(27) Fujimoto, S., and Amako, K. (1990) Guillain-Barré syndrome and *Campylobacter jejuni* infection. *Lancet 335*, 1350.
(28) Fodje, M., Grochulski, P., Janzen, K., Labiuk, S., Gorin, J., and Berg, R. (2010) Automation of the macromolecular crystallography Beamlines at the Canadian light source. *J. Synchrotron Radiat.*, 130−132.
(29) Pflugrath, J. (1999) The finer things in X-ray diffraction data collection. *Acta Crystallogr. D55*, 1718−1725.
(30) Vagin, A., and Teplyakov, A. (2010) Molecular replacement with MOLREP. *Acta Crystallogr. D66*, 22−25.
(31) Matthews, B. W. (1968) Solvent content of protein crystals. *J. Mol. Biol. 33*, 491−497.
(32) Adams, P. D., Afonine, P. V., Bunkoczi, G., Chen, V. B., Davis, I. W., Echols, N., Headd, J. J., Hung, L.-W., Kapral, G. J., Grosse-Kunstleve, R. W., McCoy, A. J., Moriarty, N. W., Oeffner, R., Read, R. J., Richardson, D. C., Richardson, J. S., Terwilliger, T. C., and Zwart, P. H. (2010) PHENIX: A comprehensive Python-based system for macromolecular structure solution. *Acta Crystallogr. D66*, 213−221.
(33) Emsley, P., and Cowtan, K. (2004) Coot: Model-building tools for molecular graphics. *Acta Crystallogr. D60*, 2126−2132.
(34) Roberts, S. J., Morris, J. C., Dobson, R. C. J., Baxter, C. L., and Gerrard, J. A. (2004) Two complete syntheses of (S)-aspartate semi-aldehyde and demonstration that Δ^2-tetrahydroisophthalic acid is a non-competitive inhibitor of dihydrodipicolinate synthase. *Arkivoc*, 166−177.
(35) Yugari, Y., and Gilvarg, C. (1965) The condensation step in diaminopimelate synthesis. *J. Biol. Chem. 240*, 4710−4716.
(36) Hayward, S., and Berendsen, H. J. C. (1998) Systematic analysis of domain motions in proteins from conformational change: New results on citrate synthase and T4 lysozyme. *Proteins 30*, 144−154.
(37) Hayward, S., and Lee, R. A. (2002) Improvements in the analysis of domain motions in proteins from conformational change: DynDom version 1.50. *J. Mol. Graphics Modell. 21*, 181−183.
(38) Poornam, G. P., Matsumoto, A., Ishida, H., and Hayward, S. (2009) A method for the analysis of domain movements in large biomolecular complexes. *Proteins 76*, 201−212.
(39) Griffin, M. D., Dobson, R. C., Gerrard, J. A., and Perugini, M. A. (2010) Exploring the dihydrodipicolinate synthase tetramer: How resilient is the dimer-dimer interface? *Arch. Biochem. Biophys. 494*, 58−63.
(40) Voss, J. E., Scally, S. W., Taylor, N. L., Atkinson, S. C., Griffin, M. D. W., Hutton, C. A., Parker, M. W., Alderton, M. R., Gerrard, J. A., Dobson, R. C. J., Dogovski, C., and Perugini, M. A. (2010) Substrate-mediated stabilization of a tetrameric drug target reveals achilles heel in anthrax. *J. Biol. Chem. 285*, 5188−5195.
(41) Atkinson, S., Dogovski, C., Downton, M., Czabotar, P., Dobson, R. J., Gerrard, J., Wagner, J., and Perugini, M. (2013) Structural, kinetic and computational investigation of *Vitis vinifera* DHDPS reveals new insight into the mechanism of lysine-mediated allosteric inhibition. *Plant Mol. Biol. 81*, 431−446.
(42) Liang, J., Edelsbrunner, H., Fu, P., Sudhakar, P. V., and Subramaniam, S. (1998) Analytical shape computation of macro-molecules: I. Molecular area and volume through alpha shape. *Proteins 33*, 1−17.
(43) Liang, J., Edelsbrunner, H., Fu, P., Sudhakar, P. V., and Subramaniam, S. (1998) Analytical shape computation of macro-molecules: II. Inaccessible cavities in proteins. *Proteins 33*, 18−29.
(44) Ho, B. K., and Gruswitz, F. (2008) Hollow: Generating accurate representations of channel and interior surfaces in molecular structures. *BMC Struct. Biol. 8*, 49.